Arabian Journal of Chemistry (2023) **16**, 104568

King Saud University

Arabian Journal of Chemistry

www.ksu.edu.sa
www.sciencedirect.com

ORIGINAL ARTICLE

The role of Carica papaya latex bio-catalyst and thermal shock in water on synthesizing rice husk

Ngafwan Ngafwan [a,*], Marwan Effendy [a], Gatot Supangkat Samidjo [b], I. Gusti Ketut Puja [c], I.N.G. Wardana [d]

[a] *Department of Mechanical Engineering, Universitas Muhammadiyah Surakarta, Jalan Ahmad Yani Pabelan Kartasura, Surakarta 57102. Indonesia*
[b] *Department of Agrotechnology, Universitas Muhammadiyah Yogyakarta, Jalan Brawijaya, Tamantirto, Yogyakarta 55183. Indonesia*
[c] *Department of Mechanical Engineering, Universitas Sanata Dharma, Jalan Affandi, Mrican, Depok, Sleman, Yogyakarta 55281. Indonesia*
[d] *Department of Mechanical Engineering, Universitas Brawijaya, Jalan MT. Haryono, Malang 65145. Indonesia*

Received 25 June 2022; accepted 8 January 2023
Available online 13 January 2023

KEYWORDS

Amorphous material;
Bio-catalyst material;
Nanocomposites;
Carbon nanoparticles;
Rice husk

Abstract A bio-catalyst made of natural resources, such as Carica papaya latex, is very challenging for nanoparticle separation. In addition, differences in thermal conditions between nanoparticles affect the movement of substances in the separation process. The study experimentally investigated the role of Carica papaya latex bio-catalyst and thermal shock in water on synthesizing rice husk (RH). The synthesis retained the Mg and C elements attached to SiO_2, which were generally neglected during the process. The study's objective was to evaluate the effectiveness of biocatalysts and thermal effects on the separation of Mg-SiO_2-C from rice husk carbon nanoparticles (CNPs-RH). The research involved various treatment processes, such as RH pyrolysis in obtaining charcoal, High energy milling (HEM) to have carbon particles, and washing to get nano-sized carbon particles. The bonding of elemental compounds to rice husk carbon particles (CPs-RH) was released using NaOH and coagulation using a bio-catalyst. Coagulated CPs-RH was injected into water at a temperature of 60–70 °C to have a thermal shock effect for H_2O clusters in Na^+ and Mg^{2+} ions attached to the surface of the nanoparticles. Several tests were carried out, such as the SEM-EDX, TEM, XRD, and FTIR tests, to investigate the two nanoparticle clusters formed up to the nanometer scale. The results indicated that CNPs-RH nanoparticles consist of spherical particles with a diameter of 1.2 nm, while Mg-SiO_2-C nanoparticles have a diameter of 0.6 nm. Both

* Corresponding author.
E-mail address: ngafwan@ums.ac.id (N. Ngafwan).
Peer review under responsibility of King Saud University.

Production and hosting by Elsevier

https://doi.org/10.1016/j.arabjc.2023.104568

are classified as amorphous. Based on the FTIR test, CNPs-RH is hydrophilic, while Mg-SiO_2-C is hydrophobic. Thermal shock in water strengthens the ion's mobility, increasing the interfacial dipole forces between nanoparticles and accelerating the separation process.

1. Introduction

The synthesis of various natural-based materials is still being carried out to produce new nanomaterials with better physical properties and chemical functions. Efforts to develop new nanomaterials are realized by considering comprehensive aspects, freeing the material from toxic properties and suitability for material roles, and paying attention to synthesis using green production methods based on renewable materials as environmentally friendly production systems. Carbon nanoparticles (CNPs) are an attractive alternative material with several advantages compared to other existing nanoparticles. Scientifically, nanomaterials are in great demand because of their microscopic dimensions and unique physical properties.

High-quality porous material, like silica (SiO_2), has been successfully developed to the nanoscale to address the availability of energy storage technologies and various agricultural waste problems. Rice husk charcoal is a potential material to build the morphology of porous materials to the nanoscale, which can be applied in absorbing electromagnetic waves in handling organic and inorganic wastes, mainly heavy metals. Silica derived from rice husk (RH) is cost-effective and environmentally friendly. In a recent study, Silica Quantum Dots (SiO_2-QDs) made of RH could be successfully developed up to less than 10 nm (Astuti et al., 2022). This finding opens new insights into semiconductor developments, energy harvesting, and bio-imaging, including fluorescent dye application.

The remaining agricultural product in the form of RH is abundant as a sustainable and renewable energy source and can be developed to produce low-cost and environmentally friendly biomaterials. Not surprisingly, developing materials made of biomass is increasingly attractive. An experimental study noted that RH could be converted into composites such as Mg_2Si, SiO_2, SiC, and Si_3N_4 (Soltani et al., 2015). RH has great potential as a source of SiO_2 to support ion exchange at a lower price than other commercial products. This material could also be developed into an active and stable bio-catalyst in aqueous and non-aqueous media (Bolina et al., 2018).

Furthermore, SiO_2 nanoparticles derived from RH could be synthesized to improve chemical oil recovery (Agi et al., 2020). The produced SiO_2-supported CaO catalyst offers promise as a transesterification process catalyst (Lani, Ngadi and Inuwa, 2020). In comparison, SiO_2 particle made of RH is a stable bio-catalyst in esterification (Sabi et al., 2022). In another study, as bio-catalysts, SiO_2 generated from RH, i.e., without adding any foreign metal phase, facilitates a compelling hydrogen synthesis via methane breakdown (Gómez-Pozuelo et al., 2021).

In recent, the product of RH has been widely used as a construction material for concrete products (Lo, Lee and Lo, 2021)(Faried et al., 2021), as an adsorbent for organic dyes (Da Rosa et al., 2019; Khan et al., 2020; Ponce et al., 2021), and as a hazardous textile dye (Sivalingam and Sen, 2020). In addition, rice husk ash (RHA) is also helpful as an absorber of heavy metals (Basu et al., 2019; Priya et al., 2021; Tokay and Akpınar, 2021), such as Palladium Pd (Nabieh et al., 2021), Lead Pb (Babazad et al., 2021), Mercury (Zhao, Guo and Zheng, 2010), Cadmium Cd^{2+} (Zainal Abidin et al., 2020) and Zink Zn^{2+} (Priya et al., 2021). RHA is also an economical raw material for producing silicate and silicon (Flores et al., 2021). Bio-sorbents have many advantages, including recycling waste materials, removing pollutants, and reducing the need for costly chemicals, considering eco-green treatments (Usgodaarachchi et al., 2021). Unmodified RH has a low metal ion adsorption capacity (Nabieh et al., 2021).

Synthesis of SiC and carbon nanoparticles based on biomass waste such as rice husk (RH), straws, or sugarcane leaves have been widely carried out using conventional approaches that require heating at high temperatures (Chiew and Cheong, 2011). So far, the synthesis of SiC and carbon nanoparticles with natural materials or bio-catalysts is limited. Therefore, it is interesting to study the synthesis of both with bio-catalyst from Carica papaya latex to develop a new environmentally friendly technology, resulting in two benefit products, i.e., rice husk carbon nanoparticles (CNPs-RH) and magnesium silica oxide carbide (Mg-SiO_2-C). The synthesis was carried out on rice husks (agriculture wastes) with high silica content. The synthesis of both nanoparticles based on RH charcoal combined with natural active ingredients from Carica papaya latex and NaOH is expected to fill the knowledge gap. So far, the synthesis only produces silicon carbide (SiC) with weak catalyst characteristics (Soltani et al., 2015).

In a recent experimental study, Carica papaya latex bio-catalyst in water forms bio ions which trigger the release of the functional group bonds of the pulp nanoparticles (Anisa et al., 2022). However, synthesizing RH seems to produce only minor ion mobility, which only results in stretching different nanoparticle clusters, and no functional cluster termination occurs.

RH has been extensively studied to obtain microporous and mesoporous activated carbon, including extraction products such as Si, SiO_2, and SiC. Most synthetical RH product is in SiO_2, which combines with carbon. RH is commonly burned to ash and washed using KOH or NaOH to obtain activated carbon. A study noted that KOH is more effective than NaOH (Muniandy et al., 2014). Another way is that RH is made of charcoal with high-energy milling (HEM) treatment and then dissolved using KOH, followed by a filtering process to produce SiO_2.

Concerning the synthesis of CNPs from RH wastes, Carica papaya latex was investigated for its effects on production. SiO_2 could be separated from carbon charcoal without removing the carbon content. RH contains several chemical elements, such as C, O, Mg, Si, Ca, Fe, Al, and K. This research applied the role of NaOH and Carica papaya latex bio-catalyst to extract C and Si elements in the form of SiO_2, which form nanoparticle clusters by retaining Mg elements. The separation process was followed by shock heat treatment involving a Carica papaya latex bio-catalyst.

2. Materials and methods

Most of the synthetic products from rice husk (RH) were in the form of silica (SiO_2) and silicon carbide (SiC), which were usually obtained by burning them to ashes and then washing them using potassium hydroxide (KOH) or sodium hydroxide (NaOH). So far, the production of SiO_2 did not consider the Mg element, which had great potency in daily life. In the synthesis, Mg and C elements were maintained attached to SiO_2.

The bonding of the elemental compounds in CPs-RH was released using NaOH and coagulation using Carica papaya latex bio-catalyst. Coagulated CPs-RH was injected into water at a temperature of 60–70 °C to get a thermal shock effect for H_2O clusters in Na^+ and Mg^{2+} ions attached to the surface of the nanoparticles. The ion's mobility increased the interfacial dipole forces, accelerating the separation of Mg-SiO_2-C from CNPs-RH. The SEM-EDX, TEM, XRD and FTIR tests were

conducted to evaluate the effectivity of bio-catalyst derived from Carica papaya latex by investigating the two nanoparticle clusters formed up to the nanometer scale.

2.1. Materials and preparation

This study used rice husk (RH) and Carica papaya raw materials from plantations in Central Java, Indonesia. There were no treatments for RH before pyrolyzing. Bio-catalyst made of young papaya latex was realized by mixing it with 70 % alcohol, and sodium hydroxide (NaOH) was applied to break down the charcoal particles obtained from HEM.

The synthesis process is shown in Fig. 1. The first step was to pyrolyze the RH to obtain RH charcoal at 600 ^{0}C. A stainless-steel tube high energy milling (HEM) shaker mill with steel balls was used for pounding RH charcoal up to 2 million cycles. The resulting carbon was immersed in a mixed 600-gram water and 3 mol NaOH. In this step, the non-precipitated portion was separated into CPs-RH.

2.2. Dispersion and coagulation

One gram of CPs-RH was dispersed using 3 mol of sodium hydroxide (NaOH) in water (Muniandy et al., 2014). The dispersion process was carried out for 2 h. The dispersed CPs-RH in water were then coagulated by adding a Carica papaya latex bio-catalyst.

In water, this bio-catalyst formed negative-and-positive bio ions by taking a molecule of H_2O. After the formation of ions, both oxygen (O_2) and hydrogen (H_2) were released. The reaction of oxygen and Na + resulted in Na_2O, which eliminates the dipole forces between equally charged nanoparticles. Finally, the Na^+ bonds were replaced by H_2O to form the hydrogen bonds, indicating coagulation.

2.3. Separation process

Along with coagulation, the nanoparticle spacing of different properties has been stretching. The gap is noticeable due to the thermal shock from the injection process into the hot water. The process of separating nanoparticles was realized by injecting the coagulated CPs-RH into the water at a temperature of 60–70 °C. The injection process produced two clusters of nanomaterial types, namely dark brown and light brown groups, then separated and washed by water conditioned at pH up to 7.36.

2.4. Experiments and characterization

This study performed SEM-EDX (Scanning electron microscope - Energy disperse X-ray), TEM (Transmission electron microscopy), XRD (X-ray diffraction), and FTIR (Fourier transform infrared spectroscopy) test to characterize two nanoparticle clusters up to the nanometer scale. Two nanoparticles, pure CNPs-RH and Mg-SiO_2-C composite, were tested using SEM and EDX to analyze morphology, size, phase distribution, and chemical composition. The SEM test machine series is FEI inspect S-50. The TEM test was realized to investigate the specimen's morphology in-depth. The XRD test was used to identify the crystallographic structure of the synthesis products. The XRD series of testing machines is the PAN analytical X'PERT PRO. In addition, the FTIR spectroscopy test

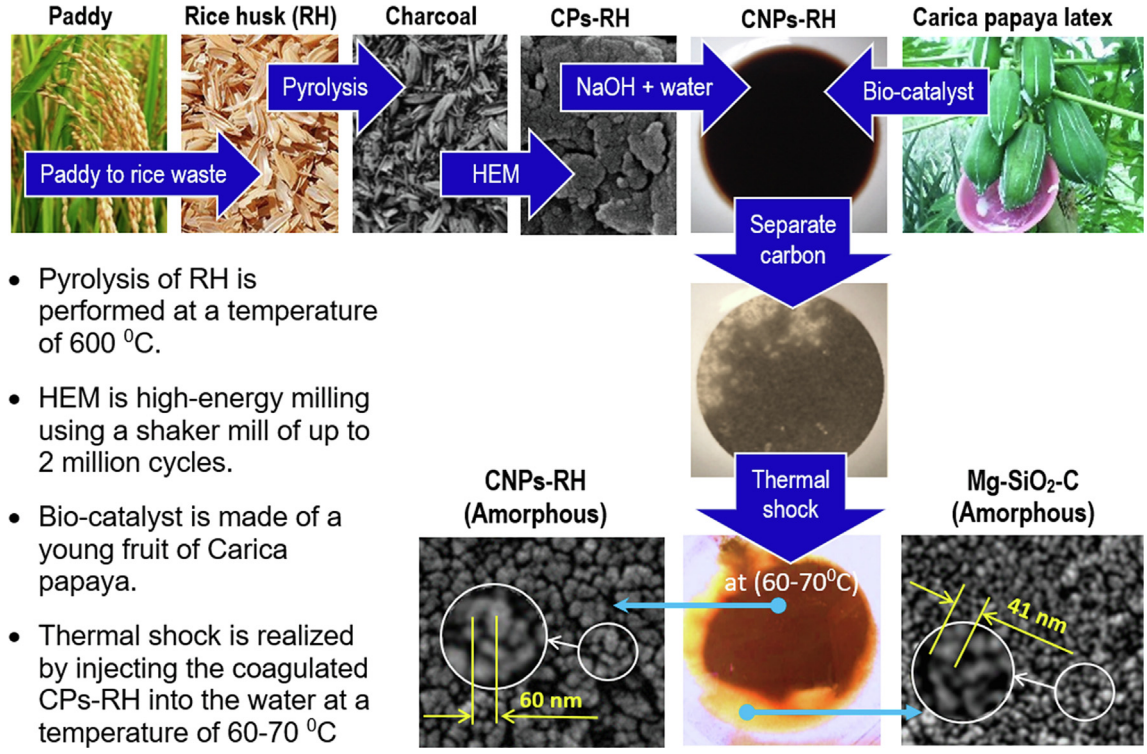

Fig. 1 The synthesis processes.

was realized to identify the changes in functional groups. FTIR testing machine is Shimadzu brand, type: Prestige 21.

3. Results and discussion

The synthesis of Mg-SiO_2-C composite from rice husk carbon (CPs-RH) has been studied analytically and experimentally. It was found that rice husk (RH) has a great potential to be amorphous nanoparticles (CNPs-RH). The Carica papaya latex bio-catalyst and thermal shock in water play a key role in separating Mg-SiO_2-C from rice husk carbon nanoparticles (CNPs-RH). The main results and a more detailed discussion are presented as follows.

3.1. Photosynthesis

Based on the basic concept of photosynthesis (Song et al., 2014), Mg^{2+} and Si^{4+} ions in rice husk react with H_2O, and CO_2 takes photon energy from the sun. Thus, the proposed Mg^{2+} photosynthesis is.

$$Mg^{2+} + 2H_2O + 2CO_2 + \text{Photon} \rightarrow 2H_2CO_3 + Mg^{2+}$$

$$Mg^{2+} + 2HCO_3^- + 2H^+ \rightarrow Mg(HCO_3)_2 + 2H^+$$

$$Mg(HCO_3)_2 + 2H^+ + H_2CO_3 \rightarrow Mg(HCO_3)_2 + 2H^+ + H^+ + HCO_3^-$$

$$Mg(HCO_3)_2 + 2H^+ + (H^+ + HCO_3^-) + CO_2 \rightarrow$$

$$Mg(HCO_3)_2 + 3H^+ + (CO(COOH))^- + O_2 \quad (1)$$

While the proposed Si^{4+} photosynthesis is.

$$Si^{4+} + 2H_2O + 2CO_2 + \text{photon} \rightarrow Si^{4+} + 2H_2C \quad O3$$

$$Si^{4+} + 4H_2CO_3^- + 2H^+ \rightarrow Si(HCO_3)_4 + 6H^+$$

$$Si(HCO_3)_4 + 6H^+ + H_2CO_3 \rightarrow Si(HCO_3)_4 + 6H^+ + H^+ + HCO_3^-$$

$$Si(HCO_3)_4 + 6H^+ + H^+ + HCO_3^- + CO_2 \rightarrow$$

$$Si(HCO_3)_4 + 7H^+ + (CO(COOH))^- + O_2 \quad (2)$$

thus, resulting in the rice bran compositions in Fig. 2.

3.2. Pyrolysis

Referring to a study (Zhang et al., 2020), the pyrolysis of RH at up to 600 ^{0}C is an exemplary process for obtaining C-RH. Based on the theoretical concept (Aktas and Morcali, 2011), the pyrolysis of $Mg(HCO_3)_2$ and $Si(HCO_3)_4$ can be proposed as follows:

$$2\ Mg(HCO_3)_2 + \text{energy} \rightarrow 2\ Mg(CO)_2 + 2H_2O + 3O_2 \quad (3)$$

$$2Si(HCO_3)_4 + \text{energy} \rightarrow 2Si(CO)_4 + 4H_2O + 6O_2 \quad (4)$$

$$4(CO(COOH)) + \text{energy} \rightarrow 8(CO) + O_2 + 2H_2O \quad (5)$$

Based on the reaction of Eqs. (3) to (5), the formation of RH carbon atoms is illustrated in Fig. 2(a).

3.3. Dispersion

Fig. 3(a) is the further process of Fig. 2(c), which is the dispersion of CPs-RH by NaOH. This inorganic compound in water plays a fundamental role in dispersing the $Mg(O{-}C)_2$ and $Si(CO)_4$ bonds from the carbon of rice husk particles (CPs-RH), as shown in Fig. 2(b) and (c). The reaction product has polar properties in the atomic splitting reaction $Mg(O{-}C)_2$, as shown in Fig. 3(a).

Referring to the study of the NaOH activation process for activated sugarcane bagasse hydro char to remove dyes and antibiotics (Jais et al., 2021), the reaction can be described as follows:

$$Mg(O{-}C)_2 + 4NaOH \rightarrow Mg(O\text{-}Na^+)_2 + (CO\text{-}Na^+)_2 + H_2O_2 + 2H^+ \quad (6)$$

The separation reaction of $Si(O^-)_4$ compounds is a $Si(O{-}C)_4$ cluster from carbon particles,

$$2Si(O{-}C)_4 + 10NaOH \rightarrow 2(SiO_2^-)(Na^+) + 8(CO^-)(Na^+) + 3H_2O + 4H^+ \quad (7)$$

Similarly, the product has a polar property.

3.4. Coagulation

The coagulation of rice husk carbon nanoparticles (CNPs-RH) and composite clusters of Mg-SiO_2-C nanoparticles by bio-

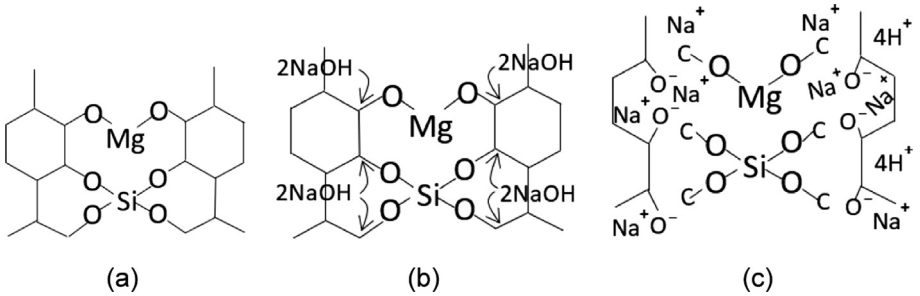

Fig. 2 The photosynthesis of rice husk. a) pyrolysis results (Si and Mg inside the rice husk). b) NaOH intervention on both Si and Mg. c) Unbonded molecular network (C—C), Mg—O, and Si—O.

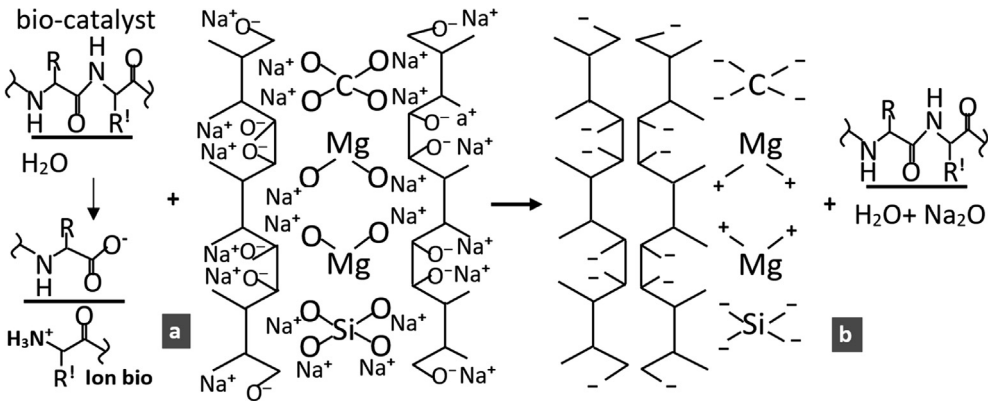

Fig. 3 Coagulation due to bio-catalyst. a) reactant. b) product.

catalysts is proposed and illustrated in Fig. 3. The bio cluster with a negative pole as an oxygen ion donor (O^-) in the carbon (C), silicon (Si), and magnesium (Mg), as given in Fig. 3(a). This cluster has a negative pole coupled with Na^+ ions. When it gets an oxygen ion donor (O^-) from a bio ion, it forms a Na_2O molecular cluster and C^{4+}, Si^{4+}, and Mg^{2+} ions. After this bio cluster releases oxygen ions (O^-), the bio cluster pole changes to positive. The bio cluster with a positive pole as a hydrogen ion donor (H^+) moves closer to the group with a negative pole of C, Si, and Mg, as in this study (Schechter, 2012). After getting a hydrogen ion donor (H^+) from a bio ion, it forms H_2O. If this bio cluster releases hydrogen ions (H^+), the bio cluster pole changes negatively.

These two bio-clusters with positive and negative poles react in water and recombine into bio-catalysts. Accordingly, the process produces H_2O, Na_2O, Si^{4+}, Mg^{2+}, and C^{4+} ions. This reaction repeatedly occurs due to the role of bioactivation until Mg^{2+}, Si^{4+}, and C^{4+} ions form oxidation in water, as illustrated in Fig. 4(a). Fig. 4(b) shows that the reaction products have two colors. This phenomenon demonstrates that the CNPs-RH cluster is dark brown, and the Mg-SiO_2-C cluster is light brown. The dispersion process of the two clusters is obvious.

3.5. The effect of thermal shock

In normal conditions, the separation of nanoparticles CNPs-RH and Mg-SiO_2-C was carried out by thermal shock treatments with a slow injection into the water at a temperature of 60–70 °C. It is intended to provide additional potential energy for Na^+ and Mg^{2+} ions. It is known that Na^+ has an ion radius of $0.095^{(+1)}$ nm, a Vander Waals radius of 0.196 nm, and a standard potential of −2.71 V. In the water, Na^+ forms clusters with hydrogen bonds (H_2O)-(H_2O)-(H_2O), which can then be formulated as [Na + $(H_2O)_n$ (n = 1–6)]. The interaction of the dipole ions exerts an influence on the order of the conjunctions, producing vibrations.

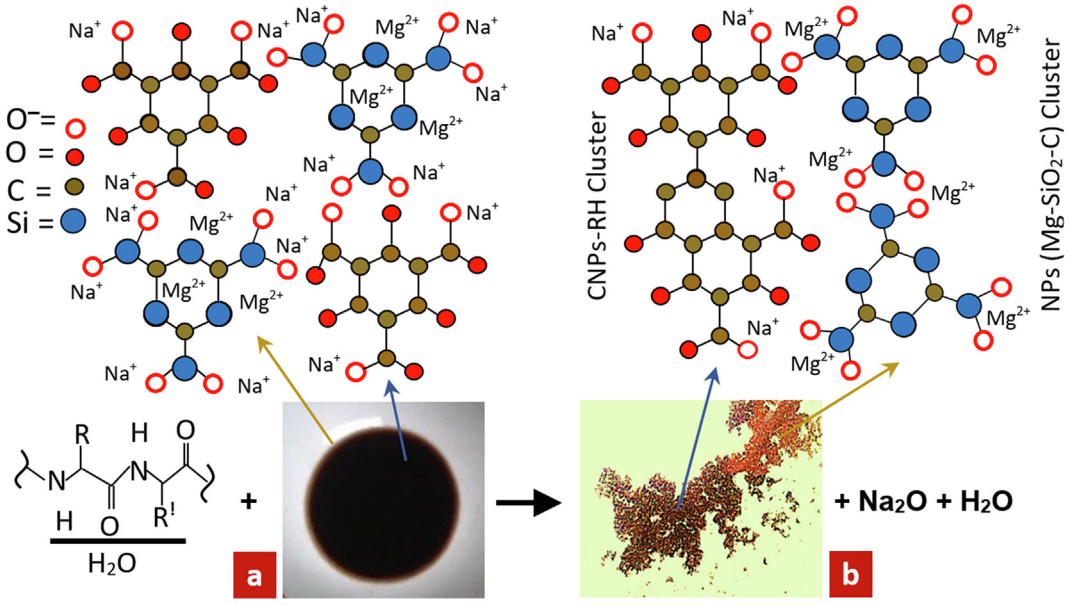

Fig. 4 The effect of Carica papaya latex bio-catalyst on nanoparticle molecular clusters. a) CPs-RH with NaOH. b) coagulation product of CNPs-RH and Mg-SiO_2-C cluster.

Meanwhile, Mg^{2+} has an ion radius of $0.065^{(+2)}$ nm, a Vander Waals radius of 0.16 nm, and a common potential −2.34 V. Mg^{2+} and hydrogen bonds (H_2O)-(H_2O)-(H_2O) to form $[Mg(H_2O)_n]^+$. Evaporation causes a change in the compound $[Mg(H_2O)_n]^+$ to $[Mg(H_2O)_{n\text{-}m}]^+ + (H_2O)_m$, while the dissociation process causes the compound $[Mg(H_2O)_n]^+$ to process into $[MgOH(H_2O)_{n\text{-}m\text{-}1}]^+ + (H_2O)_m + H$. The interaction of the dipole ions gives a conjunction sequence, which then produces vibrations. It means that both of them have mutually pushing forces between the two clusters [Na + $(H_2O)_n$ (n = 1–6)] attached to the RH-CNPs and [Mg $(H_2O)_n]^+$ attached to SiO_2-C, as in Fig. 4(b).

Thermal shock treatment by injecting it into the water at a temperature of (60–70) °C aims to increase the energy of Na^+ and Mg^{2+} ions in forming clusters with water to form larger groups. In a study (Stachl and Williams, 2020), the increase in cluster dimensions has a vital role in increasing the amount of vibration energy so that it then produces a greater force and finally can separate two types of clusters [$Na^+(H_2O)_n$ (n = 1–6)] attached to the dark brown CNPs-RH and [Mg $(H_2O)_n]^+$ attached to SiO_2-C is light brown. Under dry conditions, it produces CNPs- RH, and Mg-SiO_2-C, as shown in Fig. 5.

In Fig. 5(a), the CNPs-RH cluster can bind H_2O to form Vander Waals bonds on carbon nanoparticles, namely (H_2O)-(O—C—C_6-C_6—C—O), which is hydrophilic. As in Fig. 5(b), Mg-SiO_2-C in the MgO bond does not form a Vander Waals bond; therefore, it is hydrophobic.

3.6. Morphology and surface phase composition

Fig. 6 exhibits the surface morphology of rice husk based on SEM and TEM testing. Fig. 6(a) indicates the SEM result of rice-husk carbon (CPs-RH) before dispersing by NaOH and Carica papaya latex bio-catalyst. NaOH triggers the dispersal of nanoparticles, whereas the Carica papaya latex causes the coagulation of nanoparticles inside the water. As in the study (Stachl and Williams, 2020), the presence of thermal shock increases the polar strength on the surface, which can separate CNPs-RH and Mg-SiO_2-C, as shown in Fig. 6(b) and 6(c), respectively. The TEM tests are available in Fig. 6 (b_1-b_3) and Fig. 6 (c_1-c_3) to magnify their morphologies. In detail, it can be observed up to 5 nm.

From Fig. 6(a), it was observed that the carbon surface which collides with the steel ball in the high-energy milling process forms nanometer-scale fractures. These fractures are nano cracks containing residual stress, which causes a weakening of the bond energy of the compound. NaOH in water is used to break down carbon particles into nanoparticles. The entered hydroxyl ions OH^- and Na^+ in the fracture play a role in the attachment process to the fracture wall, which results in the fracture wall becoming polar. Similar to this study (Gao et al., 2022), the polar nature of the fracture wall results in a dipole force between the walls. It provides a moment at the crack tip containing residual stress. As a result, the crack propagation coincides with the entire carbon surface in the residual stress area.

The SEM test shows the morphology of CNPs-RH under 100 nm and Mg-SiO_2-C under 50 nm in Fig. 6(b) and (c), respectively. A TEM test was carried out to validate the nanoparticles, as shown in Fig. 6(b_1) and 6(c_1), and both nanoparticle sizes are offered to reach less than 100 nm. The TEM test up to 20 nm in size, as shown in Fig. 6(b_2) and 6 (c_2), indicates tiny nanoparticle grains that are not visible. From the magnification of the TEM test image, it can be seen that these small grains yield up to 1.2 nm for CNPs-RH and 0.6 nm for Mg-SiO_2-C.

Fig. 7 shows the results of the XRD test for CPs-RH, CNPs-RH, and Mg-SiO_2-C. The composition of the amorphous and crystalline phases is visible. The area of the amorphous phase on the carbon particles of CPs-RH is 1,842, about 84.6 %, while the crystalline phase of $C_2CaO_4{\cdot}H_2O$ is 336, equivalent to 15.4 %. The crystalline phase is at positions 2θ = 29.37. The area of the amorphous phase on the CNPs-RH carbon nanoparticles is 719.4, approximately 78.8 %, while the crystalline phase of $CaCO_3$ is 193.8, equivalent to 21.2 %. The crystalline phase is at position 2θ = 29.39. The area of the amorphous phase of the Mg-SiO_2-C nanoparticles is 719.4, approximately 81.4 %, and the $CaCO_3$ crystalline phase is 164.5, equivalent to 18.6 %. The crystalline phase is at position 2θ = 29.43. Based on the results of the XRD test, the material obtained in the study is amorphous.

Table 1 gives the chemical compositions of CPs-RH, CNPs-RH, and Mg-SiO_2-C based on the EDX test. It was found that the dominant ingredients are C, O, Mg, Si, and Ca. The per-

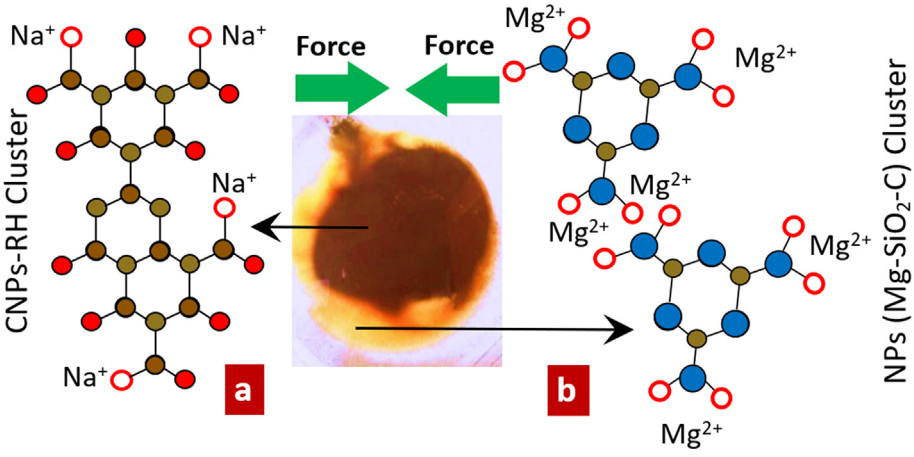

Fig. 5 The effects of thermal shock on both clusters of CNPs-RH and Mg-SiO_2-C. a). The dark brown CNPs-RH cluster. b). The light brown Mg-SiO_2-C cluster.

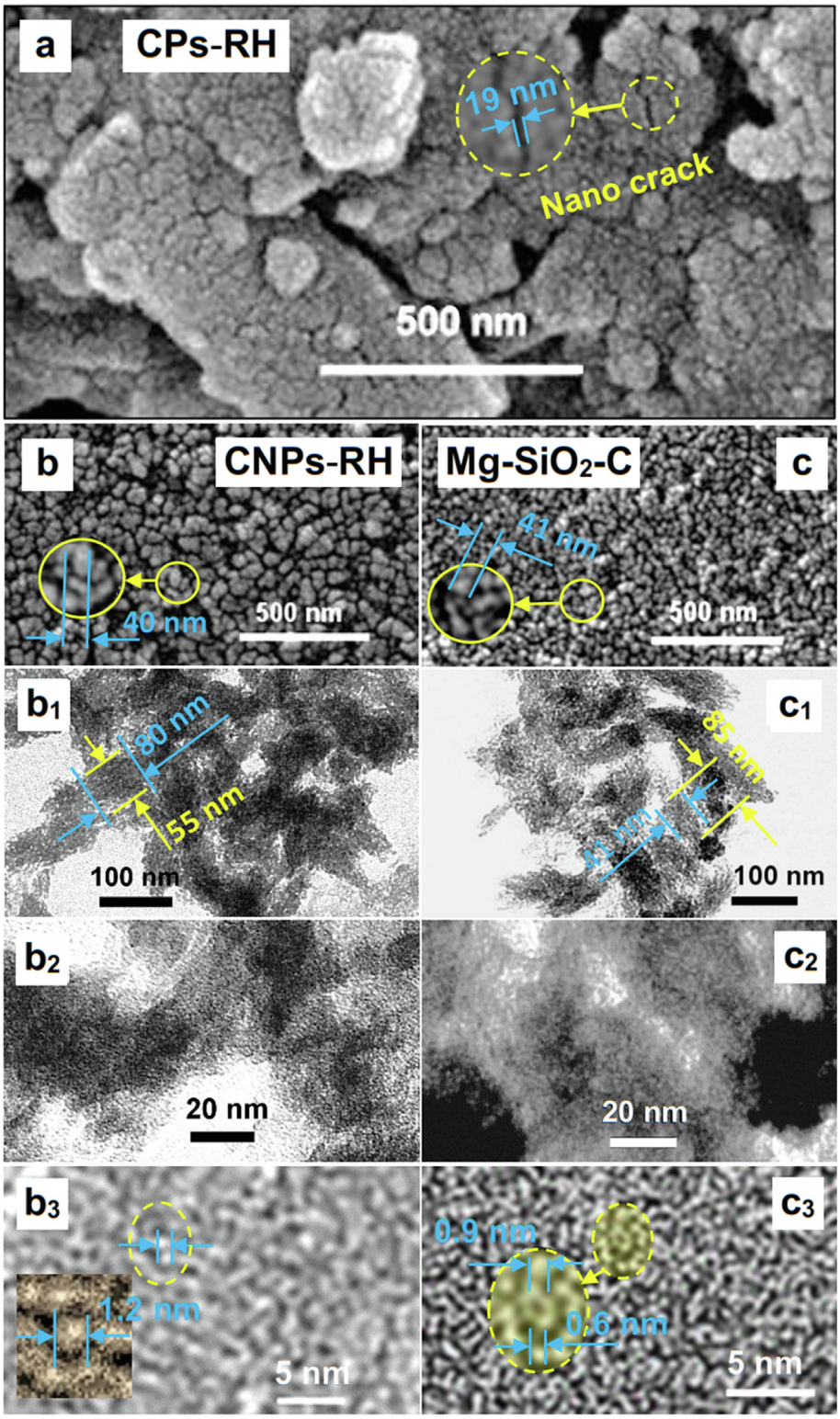

Fig. 6 The role of Carica papaya latex bio-catalyst in synthesizing CPs-RH. (a) SEM of CPs-RH, (b) SEM of CNPs-RH, (c) SEM of Mg-SiO_2-C, (b_1-b_3) TEM of CNPs-RH, (c_1-c_3) TEM of Mg-SiO_2-C.

centage of Ca atoms is 8.35 % in Mg-SiO_2-C. The percentage of weight and atoms changes after being injected into water at a temperature of around 60–70 °C. These changes follow the XRD test results, where the Ca atoms form crystals of $CaCO_3$ and CaC_2 in CNPs-RH and $CaCO_3$ in Mg-SiO_2-C. It means that 100 atoms have 8Ca atoms, which require 8C atoms and 24O atoms to form a crystal of 8($CaCO_3$), while the rest are 16C atoms, 22O atoms, 10 Mg atoms, and 11Si atoms.

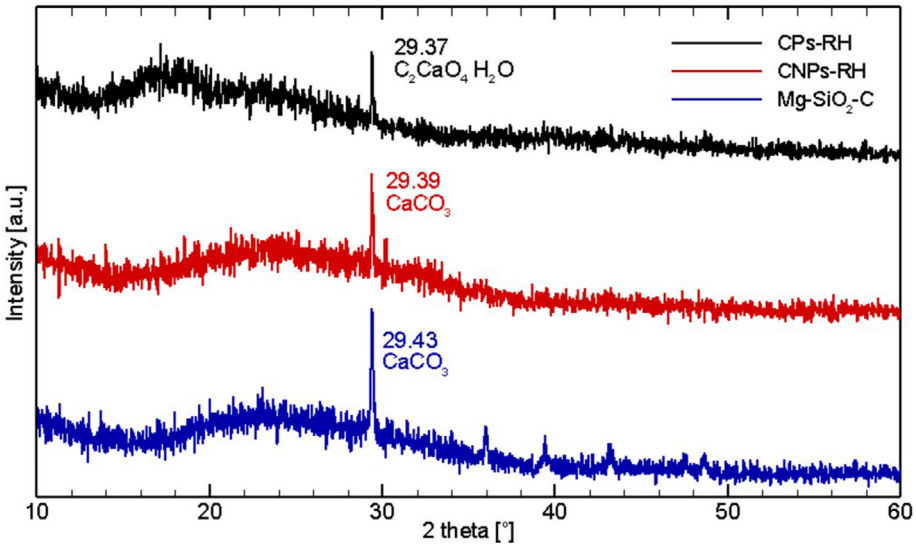

Fig. 7 The XRD pattern of CPs-RH, CNPs-RH, and Mg-SiO_2-C.

Table 1 The chemical compositions of CPs-RH, CNPs-RH and Mg-SiO_2-C.

Components	Weight (Wt%)			Atomic (At%)		
	RH	CNPs-RH	Mg-SiO_2-C	RH	CNPs-RH	Mg-SiO_2-C
C	60.74	83.01	22.68	24.00	88.64	33.19
O	19.11	11.42	38.97	46.38	9.19	42.82
Mg	0.30	1.07	14.23	10.33	0.57	10.29
Si	5.64	0.91	16.61	10.92	0.41	10.40
Ca	6.90	3.23	7.50	4.31	1.05	3.29
Fe	1.74	0.05	–	1.07	0.01	–
Al	2.72	–	–	2.52	–	–
K	2.84	–	–	0.46	–	–
P	–	0.30	–	–	0.12	–
others	0.01	0.01	0.01	0.01	0.01	0.01

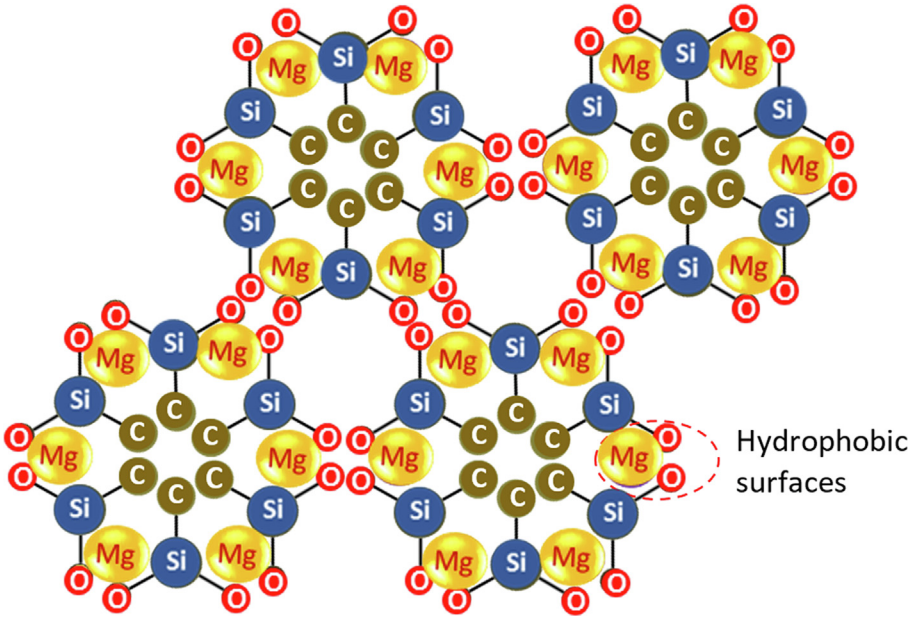

Fig. 8 The proposed molecular configuration of Mg-SiO_2-C nanoparticles resulted from CPs-RH separation.

Based on these findings, the molecular configuration of the nanoparticles formed is Mg-SiO_2-C. The remaining elements formed 10 clusters of Mg-SiO_2-C, which offer to form groups in Fig. 8. In this case, the remaining two C and Si atoms create a further chain of bonds.

The Mg element has an ion radius of $0.065^{(2+)}$ nm, Vander Waals radius of 0.16 nm, and voltage of −2.34 V in water. This configuration is hydrophobic, while the surface of CNPs-RH in water is hydrophilic, as seen in Fig. 4(b). The CNPs-RH and Mg-SiO_2-C in water can be grouped based on these two properties. Physically, the elements of Mg and Si have atomic weights greater than C. Therefore, the separation of the Mg-SiO_2-C position is below and then pushed out of the area of the CNPs-RH elements due to the high mobility of Mg. This phenomenon is shown in Fig. 5. This causes aggressive behavior, which plays a role in combining SiO_2-C, as illustrated in Fig. 8.

3.7. Identification of functional clusters

Fig. 9 shows the FTIR spectra of CPs-RH, CNPs-RH, and Mg-SiO_2-C, indicating the functional clusters. In the wave range between 1,750–4,000 cm^{-1}, the surface of the carbon nanoparticles of CPs-RH has phenol (O—H), an alkane (C—H) cluster, as indicated by the black graphic line. The nanocarbon particles of CNPs-RH have phenol (OH) and alkane (CH) clusters, and new groups appear, namely carboxyl (OH), nitrile (C≡N), and aromatic ring (C-Car), as shown by the red graphic line. Meanwhile, Mg-SiO_2-C nanoparticles have phenol (O—H), an alkane (C—H) cluster; new groups appear, namely nitrile (C≡N), alkyne (C≡H), as shown by the blue graphic line. In the wave range of 1,000–1,750 cm^{-1}, the surface of CPs-RH has amine (C—N) and carboxyl/ether/alcohol (C—O) clusters. At wavelengths less than 1,000 cm^{-1}, the groups present on the surface of CPs-RH, CNPs-RH are phenol (OH), alkenes (CH), and Mg-SiO_2-C is phenol (OH), and alkanes (CH).

The cluster areas on the surface of CPs-RH, CNPs-RH, and Mg-SiO_2-C are shown in Fig. 10. The phenol (O—H) area from 144.76 in CPs-RH, after being treated, the size of phenol (O—H) increases to 213.60, located in CNPs-RH and Mg-SiO_2-C. After treatment, the alkane area of 119.21 on CPs-RH decreases to 81.84, located in CNPs-RH and Mg-SiO_2-C. The alkene area is 53.25 in CPs-RH; after processing, it increases to 136.96, found in CNPs-RH and Mg-SiO_2-C. The C-Car aromatic ring group is 46.04 on CPs-RH; after processing, it expands to 151.98, located on CNPs-RH and Mg-SiO_2-C. After processing, ketone groups (C—O) on CPs-RH are not visible. The amine cluster area is present on CPs-RH; after processing, it is only visible on CPs-RH. Various other groups formed are carboxyl (CH), C═Ctrans, nitrile (C≡N), alkyne (C≡H), nitrile (C≡N), and ketone (C═O). Nitrile (C≡N) and ketone (C═O) appear on CNPs-RH and Mg-SiO_2-C, respectively.

The C—H alkane and alkene clusters give surface hydrophobicity. The under-peak area of Mg-SiO_2-C is more significant than that of CNPs-RH. It indicates the hydrophobic strength, as in Fig. 10. The carboxyl group O—H causes hydrophilic properties that bind to water, reducing the hydrophobic properties of CNPs-RH. Meanwhile, the C—O ether cluster gives hydrophobic properties, which increase the

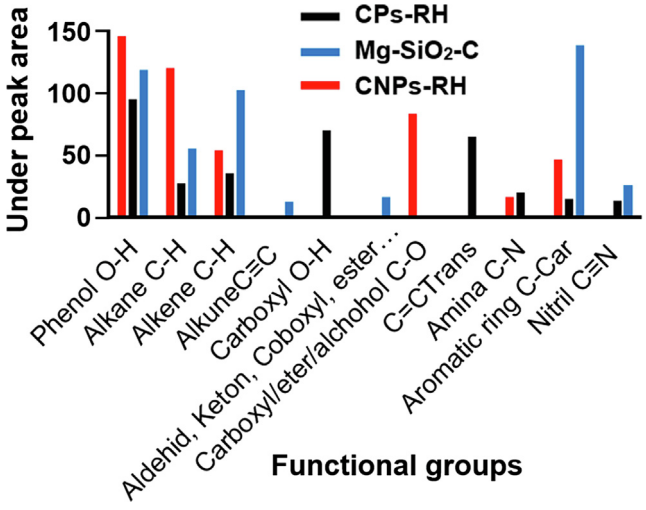

Fig. 10 The under-peak area of the functional groups.

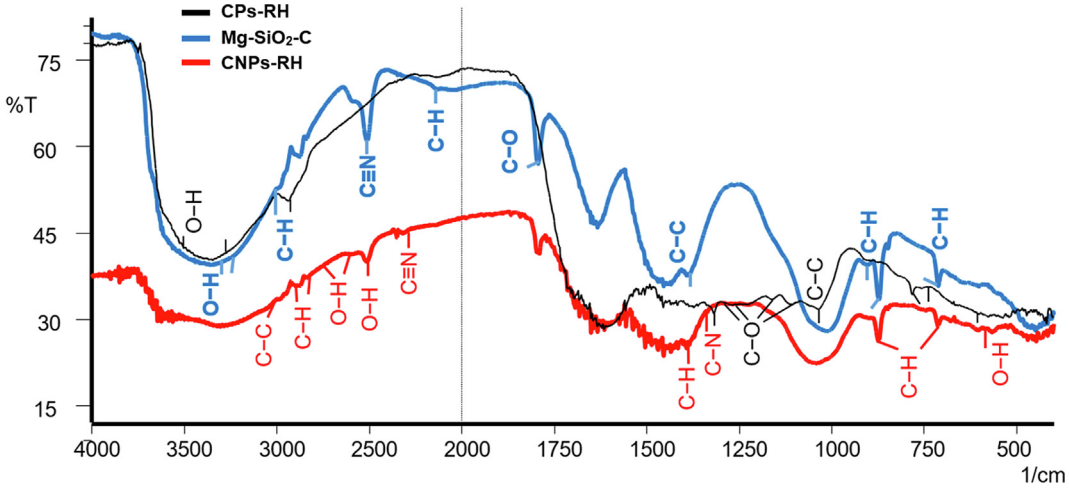

Fig. 9 The FTIR spectra of CPs-RH, CNPs-RH, and Mg-SiO_2-C.

hydrophobicity of the Mg-SiO_2-C. Therefore, Mg-SiO_2-C are hydrophobic, which has a role in separating the two nanoparticles in water.

4. Conclusion

The synthesis of CNPs-RH and Mg-SiO_2-C from rice husk carbon (CPs-RH) has been analytically and experimentally studied up to the nanoscale. The separation involved the role of NaOH and Carica papaya latex bio-catalyst. The synthesis utilized the interfacial bipolar force of the nanoparticle cluster generated by Na^+ dan Mg^{2+} ions strengthened by thermal shock during injection of CPs-RH into the water at 60–70 °C, forming two groups with different colors. Various tests were used to prove the formed nanoparticles, such as SEM-EDX, TEM, XRD, and FTIR. It can be concluded that.

1. NaOH has an essential role in breaking down CNPs-RH and Mg-SiO_2-C. NaOH plays a role in dispersing (CPs-RH) in water, dispersing through nano cracks to produce nanoparticles (CNPs-RH)(Na^+), Mg(O-Na^+)$_2$, (SiO_2^-)(Na^+) and (CO^-)(Na^+) in the water.
2. The Carica papaya latex bio-catalyst plays a vital role in the polar clustering forces of Na^+ and Mg^{2+} in water, generating interfacial dipole forces to form the dark brown CNPs-RH nanoparticles and the light brown Mg-SiO_2-C, which are distributed randomly. The interfacial dipole force is strengthened by the thermal shock of water at 60–70 °C.
3. The CNPs-RH nanoparticle grains consist of spherical particles of 1.2 nm, while the Mg-SiO_2-C grains have a size of 0.6 nm.

This finding is important because most SiO_2 extract products from rice husks have not considered Mg, which has great potential in hydrogen production for sustainable energy. In agriculture, CNPs-RH can be used in slow-releasing nitrogen elements in fertilization, while composite Mg-SiO_2-C nanoparticles can improve the quality of nutrients in foliar fertilizer production.

CRediT authorship contribution statement

Ngafwan Ngafwan: Conceptualization, Methodology, Investigation, Formal analysis, Writing – review & editing. **Marwan Effendy:** Investigation, Data curation, Validation, Visualization, Software, Writing – review & editing. **Gatot Supangkat Samidjo:** Investigation, Resources. **I. Gusti Ketut Puja:** Investigation, Data curation, Writing – original draft. **I.N.G. Wardana:** Supervision, Formal analysis, Writing – review & editing.

Acknowledgments

The authors would like to thank the "**Laboratory of Synthesis and Nanomaterial Applications**" at Universitas Muhammadiyah Surakarta Indonesia for supporting the experimental works. Also, thanks to Laboratorium Sentral Universitas Gadjah Mada Yogyakarta Indonesia and Laboratorium Terpadu Universitas Negeri Malang Indonesia for helping with the testing works.

Funding

Universitas Muhammadiyah Surakarta Indonesia supported this research via 'Hibah Integrasi Tridharma' [grant number 091/A.3-III/FT/III/2021].

References

Agi, A. et al, 2020. 'Synthesis and application of rice husk silica nanoparticles for chemical enhanced oil recovery. J. Mater. Res. Technol. Korea Institute Oriental Medicine 9 (6), 13054–13066. https://doi.org/10.1016/j.jmrt.2020.08.112.

Aktas, S., Morcali, M.H., 2011. Gold uptake from dilute chloride solutions by a Lewatit TP 214 and activated rice husk. Int. J. Mineral Process 101 (1–4), 63–70. https://doi.org/10.1016/j.minpro.2011.07.007.

Anisa, N. et al, 2022. The role of Carica papaya latex bio-catalyst in recycling of used fibre pulp. Arabian J. Chem. 15, (7). https://doi.org/10.1016/j.arabjc.2022.103952 103952.

Astuti, E.S. et al, 2022. Synthesis, characterization and energy gap of silica quantum dots from rice husk. Bioresource Technol. Rep. 20, (167). https://doi.org/10.1016/j.biteb.2022.101263 101263.

Babazad, Z. et al, 2021. Efficient removal of lead and arsenic using macromolecule-carbonized rice husks. Heliyon. Elsevier Ltd 7 (3), e06631. https://doi.org/10.1016/j.heliyon.2021.e06631.

Basu, H. et al, 2019. Humic acid coated cellulose derived from rice husk: a novel biosorbent for the removal of Ni and Cr. J. Water Process Eng. 32,. https://doi.org/10.1016/j.jwpe.2019.100892 100892.

Bolina, I.C.A. et al, 2018. Preparation of ion-exchange supports via activation of epoxy-SiO_2 with glycine to immobilize microbial lipase – Use of biocatalysts in hydrolysis and esterification reactions. Int. J. Biol. Macromol. 120, 2354–2365. https://doi.org/10.1016/j.ijbiomac.2018.08.190.

Chiew, Y.L., Cheong, K.Y., 2011. A review on the synthesis of SiC from plant-based biomasses. Mater. Sci. Eng. B: Solid-State Mater. Adv. Technol. 176 (13), 951–964. https://doi.org/10.1016/j.mseb.2011.05.037.

Da Rosa, M.P. et al, 2019. A new approach to convert rice husk waste in a quick and efficient adsorbent to remove cationic dye from water. J. Environ. Chem. Eng. 7, (6). https://doi.org/10.1016/j.jece.2019.103504 103504.

Faried, A.S. et al, 2021. The effect of using nano rice husk ash of different burning degrees on ultra-high-performance concrete properties. Construct. Build. Mater. 290,. https://doi.org/10.1016/j.conbuildmat.2021.123279 123279.

Flores, C.G. et al, 2021. Synthesis of potassium zeolite from rice husk ash as a silicon source. Cleaner Eng. Technol. 4,. https://doi.org/10.1016/j.clet.2021.100201 100201.

Gao, X. et al, 2022. Developing Dipole-scheme heterojunction photocatalysts. Appl. Surf. Sci. 599, (6). https://doi.org/10.1016/j.apsusc.2022.153942 153942.

Gómez-Pozuelo, G. et al, 2021. Hydrogen production by catalytic methane decomposition over rice husk derived silica. Fuel 306 (July). https://doi.org/10.1016/j.fuel.2021.121697.

Jais, F.M. et al, 2021. 'Experimental design via NaOH activation process and statistical analysis for activated sugarcane bagasse hydrochar for removal of dye and antibiotic. J. Environ. Chem. Eng. 9, (1). https://doi.org/10.1016/j.jece.2020.104829 104829.

Khan, N. et al, 2020. Hydrothermal liquefaction of rice husk and cow dung in Mixed-Bed-Rotating Pyrolyzer and application of biochar for dye removal. Bioresource Technol. 309, (March). https://doi.org/10.1016/j.biortech.2020.123294 123294.

Lani, N.S., Ngadi, N., Inuwa, I.M., 2020. New route for the synthesis of silica-supported calcium oxide catalyst in biodiesel production. Renew. Energy 156, 1266–1277. https://doi.org/10.1016/j.renene.2019.10.132.

Lo, F.C., Lee, M.G., Lo, S.L., 2021. Effect of coal ash and rice husk ash partial replacement in ordinary Portland cement on pervious concrete. Construct. Build. Mater. 286,. https://doi.org/10.1016/j.conbuildmat.2021.122947 122947.

Muniandy, L. et al, 2014. The synthesis and characterization of high purity mixed microporous/mesoporous activated carbon from rice

husk using chemical activation with NaOH and KOH. Microporous Mesoporous Mater. 197, 316–323. https://doi.org/10.1016/j.micromeso.2014.06.020.

Nabieh, K.A. et al, 2021. Chemically modified rice husk as an effective adsorbent for removal of palladium ions. Heliyon 7 (1), e06062.

Ponce, J. et al, 2021. 'Alkali pretreated sugarcane bagasse, rice husk and corn husk wastes as lignocellulosic biosorbents for dyes', *Carbohydrate Polymer Technologies and Applications*. Elsevier Ltd 2,. https://doi.org/10.1016/j.carpta.2021.100061 100061.

Priya, A.K. et al, 2021. Investigation of mechanism of heavy metals (Cr^{6+}, Pb^{2+} & Zn^{2+}) adsorption from aqueous medium using rice husk ash: kinetic and thermodynamic approach. Chemosphere 286,. https://doi.org/10.1016/j.chemosphere.2021.131796 131796.

Sabi, G.J. et al, 2022. Decyl esters production from soybean-based oils catalyzed by lipase immobilized on differently functionalized rice husk silica and their characterization as potential biolubricants. Enzyme Microbial Technol. 157 (January). https://doi.org/10.1016/j.enzmictec.2022.110019.

Schechter, I., 2012. Reprint of ''On the size of the active site in proteases. I. Papain''. Biochem. Biophys. Res. Commun. 425 (3), 497–502. https://doi.org/10.1016/j.bbrc.2012.08.015.

Sivalingam, S., Sen, S., 2020. Rice husk ash derived nanocrystalline ZSM-5 for highly efficient removal of a toxic textile dye. J. Mater. Res. Technol. 9 (6), 14853–14864. https://doi.org/10.1016/j.jmrt.2020.10.074.

Soltani, N. et al, 2015. Review on the physicochemical treatments of rice husk for production of advanced materials. Chem. Eng. J. 264, 899–935. https://doi.org/10.1016/j.cej.2014.11.056.

Song, A. et al, 2014. The effect of silicon on photosynthesis and expression of its relevant genes in rice (Oryza sativa L.) under high-zinc stress. PLoS ONE 9 (11), 1–21. https://doi.org/10.1371/journal.pone.0113782.

Stachl, C.N., Williams, E.R., 2020. Effects of temperature on Cs (HO) clathrate structure. J. Phys. Chem. Lett. 11 (15), 6127–6132. https://doi.org/10.1021/acs.jpclett.0c01554.

Tokay, B., Akpınar, I., 2021. A comparative study of heavy metals removal using agricultural waste biosorbents. Bioresource Technol. Rep. 15. https://doi.org/10.1016/j.biteb.2021.100719.

Usgodaarachchi, L. et al, 2021. Synthesis of mesoporous silica nanoparticles derived from rice husk and surface-controlled amine functionalization for efficient adsorption of methylene blue from aqueous solution. Curr. Res. Green Sustainable Chem. 4,. https://doi.org/10.1016/j.crgsc.2021.100116 100116.

Zainal Abidin, N.H. et al, 2020. The effect of functionalization on rice-husks derived carbon quantum dots properties and cadmium removal. J. Water Process Eng. 38,. https://doi.org/10.1016/j.jwpe.2020.101634 101634.

Zhang, S. et al, 2020. 'Synthesis and characterization of rice husk-based magnetic porous carbon by pyrolysis of pretreated rice husk with $FeCl_3$ and $ZnCl_2$. J. Analytical Appl. Pyrolysis 147, (2). https://doi.org/10.1016/j.jaap.2020.104806 104806.

Zhao, P., Guo, X., Zheng, C., 2010. Removal of elemental mercury by iodine-modified rice husk ash sorbents. J. Environ. Sci. The Research Centre for Eco-Environ. Sci., Chinese Acad. Sci. 22 (10), 1629–1636. https://doi.org/10.1016/S1001-0742(09)60299-0.